JACS
JOURNAL OF THE AMERICAN CHEMICAL SOCIETY
Article
pubs.acs.org/JACS

Oxyfunctionalization with Cp*Ir^{III}(NHC)(Me)(Cl) with O_2: Identification of a Rare Bimetallic Ir^{IV} μ-Oxo Intermediate

Matthew C. Lehman,[‡] Dale R. Pahls,[†] Joseph M. Meredith,[§] Roger D. Sommer,[‡] D. Michael Heinekey,[§] Thomas R. Cundari,[†] and Elon A. Ison*[,‡]

[‡]Department of Chemistry, North Carolina State University, 2620 Yarbrough Drive, Raleigh, North Carolina 27695-8204, United States

[†]Department of Chemistry, Center for Advanced Scientific Computing and Modeling (CASCaM), University of North Texas, Denton, Texas 76203, United States

[§]Department of Chemistry, University of Washington, Box 351700, Seattle, Washington 98195-1700, United States

Supporting Information

ABSTRACT: Methanol formation from [Cp*Ir^{III}(NHC)Me(CD$_2$Cl$_2$)]$^+$ occurs quantitatively at room temperature with air (O_2) as the oxidant and ethanol as a proton source. A rare example of a diiridium bimetallic complex, [(Cp*Ir(NHC)Me)$_2$(μ-O)][(BAr$^F{}_4$)$_2$], **3**, was isolated and shown to be an intermediate in this reaction. The electronic absorption spectrum of **3** features a broad observation at ~660 nm, which is primarily responsible for its blue color. In addition, **3** is diamagnetic and can be characterized by NMR spectroscopy. Complex **3** was also characterized by X-ray crystallography and contains an Ir^{IV}−O−Ir^{IV} core in which two d^5 Ir(IV) centers are bridged by an oxo ligand. DFT and MCSCF calculations reveal several important features of the electronic structure of **3**, most notably, that the μ-oxo bridge facilitates communication between the two Ir centers, and σ/π mixing yields a nonlinear arrangement of the μ-oxo core (Ir−O−Ir ~ 150°) to facilitate oxygen atom transfer. The formation of **3** results from an Ir oxo/oxyl intermediate that may be described by two competing bonding models, which are close in energy and have formal Ir−O bond orders of 2 but differ markedly in their electronic structures. The radical traps TEMPO and 1,4-cyclohexadiene do not inhibit the formation of **3**; however, methanol formation from **3** is inhibited by TEMPO. Isotope labeling studies confirmed the origin of the methyl group in the methanol product is the iridium−methyl bond in the [Cp*Ir(NHC)Me(CD$_2$Cl$_2$)][BAr$^F{}_4$] starting material. Isolation of the diiridium-containing product [(Cp*Ir(NHC)Cl)$_2$][(BAr$^F{}_4$)$_2$], **4**, in high yields at the end of the reaction suggests that the Cp* and NHC ligands remain bound to the iridium and are not significantly degraded under reaction conditions.

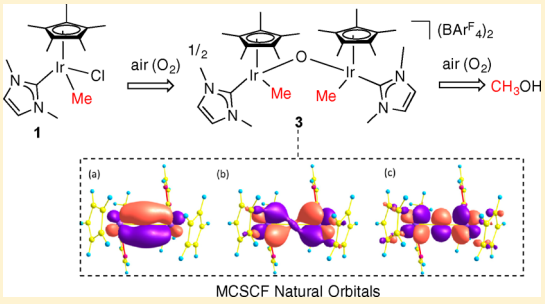

INTRODUCTION

To develop catalysts that employ molecular oxygen/air as an oxidant for the oxidation of hydrocarbons, it is important to understand the mechanism of the direct insertion of dioxygen into transition metal carbon and hydrogen bonds.[1] The mechanism for C−H activation has been well established over the past 40 years.[2] In contrast, mechanisms for oxygen insertion with O_2 are not well developed. Further, little is known about the nature of intermediates that may result from initial O_2 insertion and the factors that lead to facile C−O bond formation from these intermediates.

The insertion of O_2 into M−H and M−R (R = alkyl) bonds to form hydroperoxy and alkylperoxy species, respectively, has been reported for Pt and Pd.[1a,3] Mechanistic studies with Pt^{IV}−H complexes revealed that O_2 insertion occurs via a radical chain pathway;[4] however, O_2 coordination and hydrogen/methyl abstraction were postulated as possible mechanistic pathways for Pd^{II}−H bonds because no rate dependence on radical traps or initiators and clean first order kinetics with respect to the metal, were observed.[3f] This proposal was further corroborated by computational studies, which indicated that H atom abstraction was the operative mechanism for O_2 insertion.[5] In the case of insertions into both Pd^{II} and Pt^{II} methyl complexes, radical chain pathways were proposed.[3b,c,6]

In contrast with the examples above with palladium and platinum, O_2 insertion into iridium hydride and alkyl bonds has rarely been observed.[7] In a recent example, O_2 insertion into an Ir^{III}−H bond was proposed to occur, but the exact nature of the reaction intermediate remains elusive.[7a] C−H oxidation via direct oxygen insertion was also proposed for Cp*Ir precatalysts. However, in these reactions, the source of oxygen is water, not O_2, and cerium ammonium nitrate (CAN) and sodium periodate were utilized as external oxidants.[8] Last, dioxygen-promoted reductive elimination of R−H bonds has been observed.[9] In these examples, iridium peroxo complexes

Received: December 18, 2014
Published: February 20, 2015

DOI: 10.1021/ja512905t
J. Am. Chem. Soc. 2015, 137, 3574−3584

that resulted from the reductive elimination of R−H were isolated.

Recently, we described a rare example of C−O bond formation (oxyfunctionalization) from an Ir−methyl bond in [Cp*Ir(NHC)(Me)L][OTf] complexes where L = pyridine, THF, and CO; NHC = 1,3,-dimethylimidazol-2-ylidene; and OTf = trifluoromethanesulfonate.[10] From kinetic studies and isotope labeling experiments it was suggested that the source of oxygen was O_2 and the reaction proceeded by ligand dissociation of the L-type ligand to form a 16-electron intermediate, followed by O_2 binding and functionalization. We hypothesized that the utilization of an L-type ligand that dissociates from the metal freely at or below room temperature, could potentially allow the reaction to proceed at milder conditions and allow for the identification and isolation of relevant intermediates.

In this investigation, [Cp*Ir(NHC)Me(Cl)] has been synthesized and examined for the formation of methanol in dichloromethane with O_2 as the oxidant. We demonstrate that $NaBAr^F_4$ can be utilized to abstract the chloride ligand and generate $[Cp^*Ir(NHC)Me(CD_2Cl_2)][BAr^F_4]$ (BAr^F_4 = tetrakis[3,5-(trifluoromethyl)phenyl]borate) in situ. This complex was oxidized in the presence of air to form methanol in quantitative yields when ethanol was utilized as a proton source. A rare example of a diiridium(IV) species, $[(Cp^*Ir(NHC)Me)_2(\mu\text{-}O)][(BAr^F_4)_2]$ has been identified and shown to be a kinetically competent intermediate for methanol formation. Computational studies suggest that the μ-oxo bridge facilitates electronic communication between the iridium centers. The results presented provide insight into the nature of a critical intermediate that results from the activation of O_2 by a transition metal complex. Thus, a framework may be provided for the design of catalysts for the oxidation of hydrocarbons.

RESULTS AND DISCUSSION

Syntheses of Complexes. Previously, the formation of methanol in water from [Cp*Ir(NHC)(Me)L][OTf] (L = pyridine, THF, CO) was observed at 100 °C with O_2 (60 psi) as the external oxidant (Scheme 1).[10] It was suggested from

Scheme 1. Formation of Methanol from [Cp*Ir(NHC)(Me)L][OTf] in Water

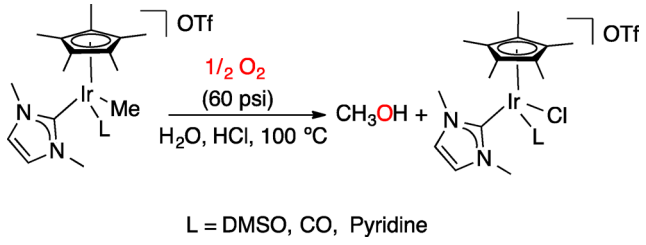

kinetic studies that the rate-determining step for this reaction involved the dissociation of the L-type ligand to form the 16-electron intermediate [Cp*Ir(NHC)(Me)][OTf]. To perform this reaction under milder conditions, we hypothesized that it may be necessary to synthesize complexes that allowed for the facile generation of this intermediate.

Complex **1**, Cp*Ir(NHC)MeCl, was synthesized from the reaction of $Cp^*Ir(NHC)Cl_2$ (NHC = 1,3,-dimethylimidazol-2-ylidene) with 0.6 equiv of dimethyl zinc and characterized by ^1H and ^{13}C NMR spectroscopy (Scheme 2). The addition of two equivalents of $NaBAr^F_4$ resulted in the quantitative formation of **2**, $[Cp^*Ir(NHC)Me(CD_2Cl_2)][BAr^F_4]$.[11]

Scheme 2. Syntheses of Complexes 1 and 2

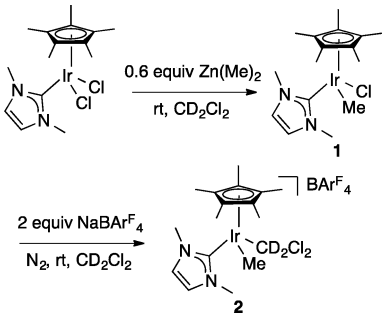

When **2** was exposed to air, an immediate color change from a yellow-brown to a deep blue solution was observed. This new complex was identified as $[(Cp^*Ir(NHC)Me)_2(\mu\text{-}O)][(BAr^F_4)_2]$, **3** (Scheme 3). Formally, **3** is a rare example of

Scheme 3. Synthesis of $[(Cp^*Ir(NHC)Me)_2(\mu\text{-}O)][(BAr^F_4)_2]$, 3

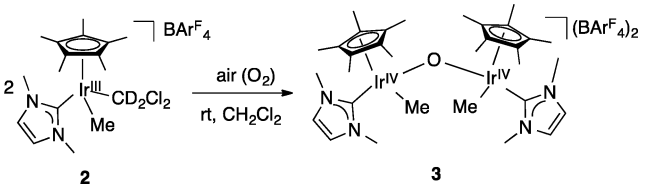

an Ir^{IV} bimetallic complex; however, complex **3** is diamagnetic and can be characterized by NMR spectroscopy (see Supporting Information). Compound **3** is stable in the solid state; however, in solution at room temperature, **3** decomposes to an unidentified iridium species over the course of 10 min (see Supporting Information).

The electronic absorption spectrum of **3** was obtained (see Supporting Information). The main features of the absorption spectrum are a broad absorption at ~660 nm (this peak is primarily responsible for the blue color) as well as absorptions at ~450, 360, and 309 nm. Strong, broad absorptions in the visible range (400−700 nm) are often seen in complexes containing a bridging μ-oxo ligand.[12] For example, the well-known compound $[(bipy)_2(H_2O)Ru^{III}(\mu\text{-}O)Ru^{III}(H_2O)(bipy)_2]^{4+}$, which also contains two d^5 metal centers, has a λ_{max} of ~640 nm.[12a] Furthermore, Crabtree and co-workers and others have reported a series of μ-oxo Ir complexes with absorptions in this range.[12f−h,13]

Structure of 3. X-ray quality crystals of **3** were obtained from the slow diffusion of pentane into a concentrated methylene chloride solution of **3** at −40 °C (Figure 1). Complex **3** consists of two half sandwich d^5 Ir(IV) centers bridged by an oxygen atom. These types of complexes are exceedingly rare: $(xylyl)_3Ir-O-Ir(xylyl)_3$ (xylyl = 2,6-$Me_2C_6H_3$) is the only other example of which we are aware.[14] In this molecule, the compound crystallizes on a 3-fold axis with the bridging oxygen on the inversion center; this results in a strictly linear (180°) Ir−O−Ir bond. By comparison, the Ir−O−Ir bond angle in **3** is approximately 150°; this deviation from linearity most likely results from steric crowding

DOI: 10.1021/ja512905t
J. Am. Chem. Soc. 2015, 137, 3574−3584

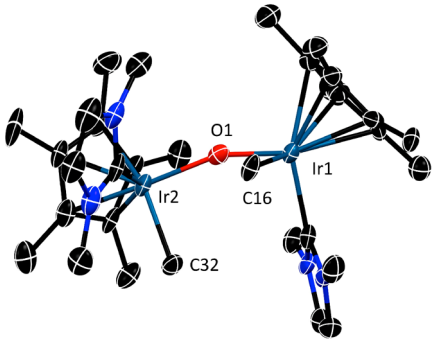

Figure 1. Thermal ellipsoid plot of $[(Cp^*Ir(NHC)Me)_2(\mu\text{-}O)]^{2+}$, **3**, (50% ellipsoids). Hydrogen atoms and the BAr^F_4 counteranions were removed for clarity. Selected bond lengths (Å) and angles (deg): Ir2–O1, 1.935; Ir1–O1, 1.934; Ir1–C16, 2.091; Ir2–C32, 2.105; Ir1–O1–Ir2, 149.60; C16–Ir1–Ir2–C32, −71.97.

around the Ir centers arising from the bulky Cp* and NHC ligands (see Supporting Information).

The Ir–O distance in **3** (1.935 Å) is consistent with a bridging oxo ligand, which range from 1.902 to 2.139 Å,[15] as opposed to $Ir_2(\mu$-hydroxo$)$[15d,16] and $Ir_2(\mu$-alkoxo$)$[17] ligands which range from 2.059 to 2.145 Å and 2.078 to 2.160 Å respectively.

Formation of Methanol. Methanol formation was not observed during the reaction outlined in Scheme 3. However, the addition of a proton source could facilitate the release of the methanol product. Methanol formation with **1** was thus attempted with a variety of acids and alcohols (acetic acid, ethanol, and phenol). The use of ethanol as a proton source resulted in quantitative yields of methanol in 1 h at room temperature. No methanol product was observed with acetic acid, and methanol yields were significantly attenuated (~15%) when phenol was used as a proton source.

Quantitative methanol yields were observed in 30 min when the reaction conditions were optimized further and the reaction was performed open to air. Thus, the optimized conditions for methanol formation are depicted in Scheme 4.

Scheme 4. Optimized Conditions for the Formation of Methanol from 1

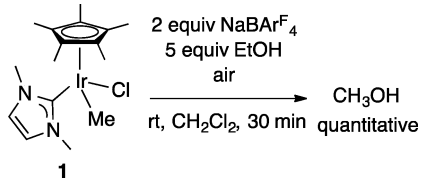

Kinetic Studies. The transformation of **2** to **3** was monitored by UV–vis spectroscopy (Figure 2). The presence of isosbestic points at 407 and 540 nm suggests that **2** is converted directly to **3** without the appreciable accumulation of any intermediates (Figure 2a). Further, when the absorbance at 660 nm was monitored over time an exponential growth for at least five half-lives was observed suggesting that the reaction exhibits a first order dependence on [**2**] (Figure 2b).

The addition of five equivalents of ethanol to **3** led to near quantitative formation of methanol (>90%) in 30 min as observed by ^{1}H NMR spectroscopy. To further confirm that **3** is an intermediate in the formation of methanol from **1**, the kinetics for the formation of methanol from **1** and **3** were

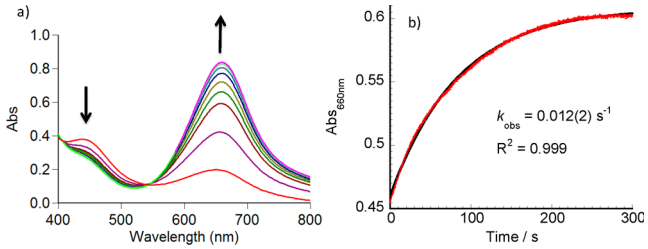

Figure 2. a) Scan of the UV–vis spectrum for the conversion of **2** to **3** vs time. Spectra were obtained every 40 s. The reaction was performed with **2** (1.0 mM), $NaBAr^F_4$ (1.2 mM) in CH_2Cl_2 in an uncapped UV–vis cell open to air at 273 K b) Time course for the conversion of **2** to **3** at 660 nm. Data are fit with nonlinear least-squares fitting to an equation describing exponential growth in Abs = a + b(1-e$^{-k_{obs}t}$).

compared. Methanol formation from **1**, over the course of 30 min followed first order kinetics and a first order rate constant, k_{obs} = 1.1(2) × 10^{-3} s^{-1} was obtained (Figure 3a). In

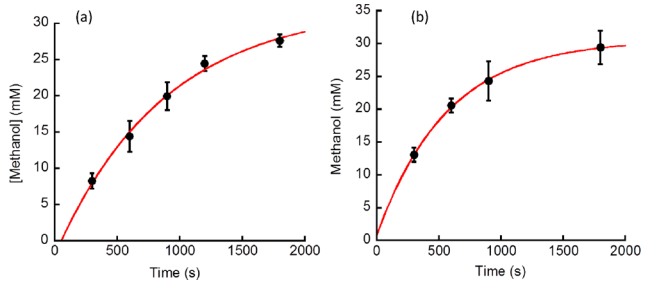

Figure 3. a) Plot of methanol formation from **1** vs time. Conditions: **1** (15 mmol, 7.1 mg); $NaBAr^F_4$ (30 mmol, 26.6 mg); C_2H_5OH (75 mmol, 4.4 μL) in 0.5 mL CD_2Cl_2 open to air at room temperature. Reactions were monitored by ^{1}H NMR spectroscopy with 1,3,5-trimethoxybenzene as an internal standard; b) Plot of methanol formation from **3** vs time. Conditions: **3** (7.5 mmol, 19.7 mg); C_2H_5OH (75 mmol, 4.4 μL) in 0.5 mL CD_2Cl_2 open to air at room temperature. Reactions were monitored by ^{1}H NMR spectroscopy with 1,3,5-trimethoxybenzene as an internal standard. Data are fit with nonlinear least-squares fitting to an equation describing exponential growth in [Methanol] = a + b(1-e$^{-k_{obs}t}$).

comparison, methanol formation from **3** resulted in a first order rate constant, k_{obs} = 1.7(2) × 10^{-3} s^{-1} (Figure 3b). The k_{obs} values suggest that **3** is a kinetically competent intermediate in this reaction.

The intermediacy of **3** was investigated further by obtaining activation parameters for the formation of methanol from both **1** and **3** according to the Eyring equation. Reactions were performed at 0, 10, and 25 °C (Figure 4). Entropically, the formation of methanol from both 1 and 3 is unfavorable ($\Delta S^{\ddagger}$ = −46(11) and −37(9) eu, respectively). The enthalpic component of the activation energy is small and positive ($\Delta H^{\ddagger}$ = 8(2) and 10(3) kcal/mol respectively), which is consistent with the observed room temperature reactivity for both complexes. When combined with the observed rate constants discussed previously, the relative activation energies provide additional evidence for the intermediacy of complex **3** in the formation of methanol from **1**.

Studies with Radical Traps. To determine if the formation of methanol occurs via a radical pathway, reactions were performed in the presence of radical traps. Reactions with **1** were performed under the conditions outlined in Scheme 4 with the radical trap TEMPO (2,2,6,6′-tetramethylpiperadin-1-

DOI: 10.1021/ja512905t
J. Am. Chem. Soc. 2015, 137, 3574–3584

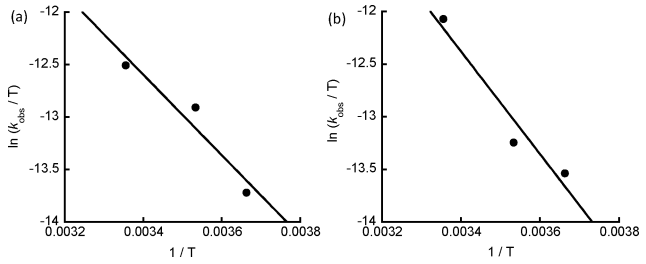

Figure 4. a) Eyring plot for the formation of methanol from **1** at 273, 283, and 298 K. Conditions: **1** (15 mmol, 7.1 mg); $NaBAr^F_4$ (30 mmol, 26.6 mg); C_2H_5OH (75 mmol, 4.4 μL) in 0.5 mL CD_2Cl_2 open to air at room temperature. Reactions were monitored by ^1H NMR spectroscopy with 1,3,5-trimethoxybenzene as an internal standard; b) Eyring plot for the formation of methanol from 3 at 273, 283, and 298 K. Conditions: **3** (7.5 mmol, 19.7 mg); C_2H_5OH (75 mmol, 4.4 μL) in 0.5 mL CD_2Cl_2 open to air at room temperature. Reactions were monitored by ^1H NMR spectroscopy with 1,3,5-trimethoxybenzene as an internal standard.

yl)oxy. When 1 equiv of TEMPO was utilized, no methanol was observed after 1 h. Methanol formation from **1** in the presence of 0.1 equiv of TEMPO reached completion at ~40% yield in 2 h. The data suggest that a radical pathway is operative for methanol formation from **1**. Similar reactivity was observed for **3**. Methanol yields were inhibited when 1 equiv of TEMPO was added to the reaction (Scheme 5). 1,4-Cyclohexadiene was also

Scheme 5. Summary of Radical Trap Experiments

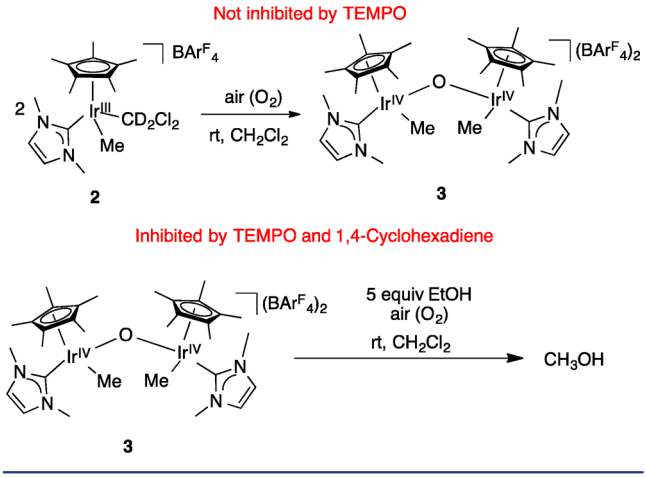

examined as a radical trap for methanol formation from **3**. When 0.5 equiv of 1,4-cyclohexadiene was added, the observed rate constant for methanol formation was reduced from k_{obs} = $1.7(2) \times 10^{-3}$ s^{-1} to k_{obs} = $7(2) \times 10^{-5}$ s^{-1}. This result, along with the reactions described previously in the presence of TEMPO, suggest that a radical pathway is operative for methanol formation.

In contrast, the formation of **3** from **2** was not affected by TEMPO. The same observed rate constant k_{obs} = 1.2×10^{-2} s^{-1} was observed when 1 equiv of TEMPO was added (see Supporting Information). Similar results were obtained when 1,4-cyclohexadiene was utilized as a radical trap. These data suggest that the formation of **3** is not inhibited by the radical trap TEMPO and imply that the formation of **3** from **2** occurs via a nonradical pathway. The results of the experiments with radical traps are summarized in Scheme 5.

Isotope Labeling Experiments and Identification of the Iridium Product. Recent reports involving complexes with Cp^*Ir^{III} frameworks have suggested that the ancillary ligands can undergo oxidative decomposition under strongly oxidizing conditions.[8c,e,12f–h,18] To determine whether the ligand framework was maintained during the formation of methanol, the origin of the methyl fragment in the methanol product was determined as well as the identity of the iridium product.

Isotope labeling studies were performed in which the methyl group bound to the iridium was labeled with deuterium. The complex **1-CD$_3$** was synthesized from $Cp^*Ir(NHC)Cl_2$ and CD_3MgBr. The presence of an Ir–CD_3 bond in **1-CD$_3$** was confirmed by ^2H NMR spectroscopy. Exposure of **1-CD$_3$** to $NaBAr^F_4$ and air resulted in the formation of **3-CD$_3$**, confirmed by ^1H, ^2H, and ^{13}C NMR spectroscopy (see Supporting Information).

The reaction of **1-CD$_3$** with $NaBAr^F_4$ and ethanol in the presence of air (Scheme 6) resulted in the formation of

Scheme 6. Isotope Labeling Studies

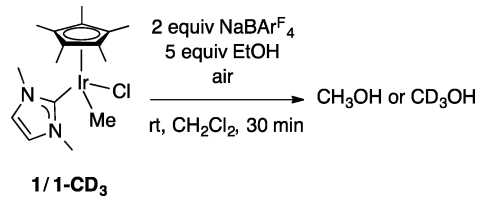

CD_3OH, as observed by ^2H NMR spectroscopy (see Supporting Information). These data are consistent with the direct oxidation of the Ir–Me bond to form methanol.

To determine whether the Cp* ligand was oxidized during the course of the reaction, the iridium product was identified. The reaction of **3** with 5 equiv of ethanol in air resulted in the identification of $[(Cp^*Ir(NHC)Cl)_2][(BAr^F_4)_2]$, **4**, in near quantitative yield (89(3)%) by ^1H NMR spectroscopy (Scheme 7).[19] X-ray quality crystals were obtained and are in agreement

Scheme 7. Isolation of 4

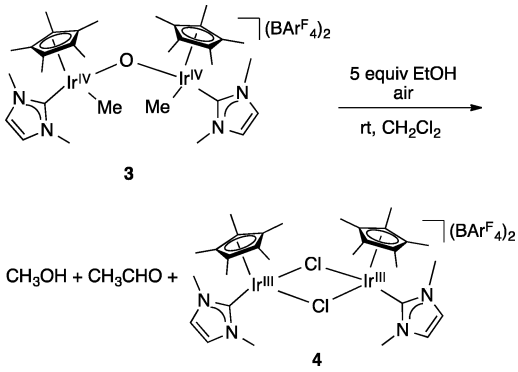

with the spectroscopic assignment of **4** as the iridium product for this reaction (see Supporting Information). Importantly, both the Cp* and NHC ligands remain intact in **4** after the oxidative conditions employed.

Role of Ethanol as a Proton Source. The role of ethanol as an additive was explored. Ethanol could potentially act as a proton source, resulting in an Ir–OEt complex, **6**, from a proposed Ir–OMe intermediate, **5**. When **3** was treated with 5

DOI: 10.1021/ja512905t
J. Am. Chem. Soc. 2015, 137, 3574–3584

equiv of ethanol in air as described in Scheme 7, acetaldehyde was observed by ^{1}H NMR spectroscopy in quantitative yields, suggesting an alkoxide exchange followed by β-hydride elimination (Scheme 8).

Scheme 8. Proposed β-hydride Elimination from an Ir−OMe Complex

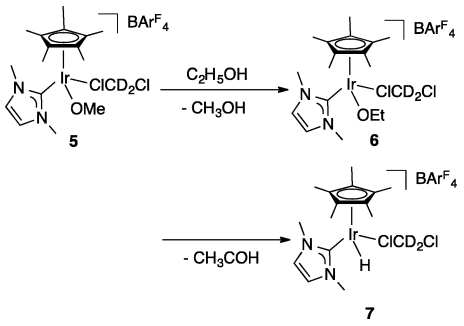

The disappearance of **3** in the presence of 5 equiv of ethanol could also be monitored by UV−vis spectroscopy at 660 nm, where **3** exhibits a strong absorbance but the product, **4**, does not. The disappearance of **3** at 660 nm follows clean first-order kinetics for at least five half-lives (see Supporting Information). Importantly, the observed rate constant, $k_{obs} = 5.2 \times 10^{-3}$ s^{-1}, is independent of the ethanol concentration. This suggests that alkoxide exchange and β-hydride elimination occurs after the rate-determining step (see Supporting Information).

Computational Studies. Computational studies were performed on some of the important species described above. For DFT (PBE0 functional) calculations, to ameliorate problems associated with calculating ionic complexes in the gas phase, calculations were performed with implicit modeling of the reaction solvent, CH_2Cl_2 (ε = 8.93), as modeled by the SMD solvation method. Addition of dispersion effects was found to be important, especially for modeling the thermodynamics of the formation of bimetallic intermediates, so these were included. Further details are given below in Computational Methods.

Activation of O_2. To understand the mechanism for the activation of O_2 by **2**, DFT calculations were performed. The proposed mechanism for the conversion for **2** to **3** is depicted in Scheme 9.

Complex **2** initially reacts with O_2 to generate the iridium dioxygen adduct, **8**. Dioxygen binding to **2** is calculated to be endergonic ($\Delta G°$ = 15.6 kcal/mol on the singlet surface and 17.4 kcal/mol on the triplet surface). Our experimental observations suggest that this step must be rate-determining because under constant O_2 pressure, the rate law for the conversion of **2** to **3** is given by (Figure 2):

$$\frac{d[\mathbf{3}]}{dt} = k_{obs}[\mathbf{2}]; \qquad k_{obs} = k[O_2]$$

Furthermore, the presence of isosbestic points at 407 and 540 nm suggests that intermediates do not accumulate in appreciable concentrations for this reaction.

Complex **8** then reacts with another molecule of **2** to generate the μ-peroxo complex **9**. This reaction is endergonic on the singlet surface ($\Delta G°$ = 32.7 kcal/mol) but much less so on the triplet surface ($\Delta G°$ = 22.3 kcal/mol). Cleavage of the O−O bond in **9** results in two oxo iridium complexes **10** ($^1\Delta G°$ = 18.8 kcal/mol, $^3\Delta G°$ = 8.7 kcal/mol)). The electronic

Scheme 9. Proposed Mechanism for the Formation of 3 from 2.[a]

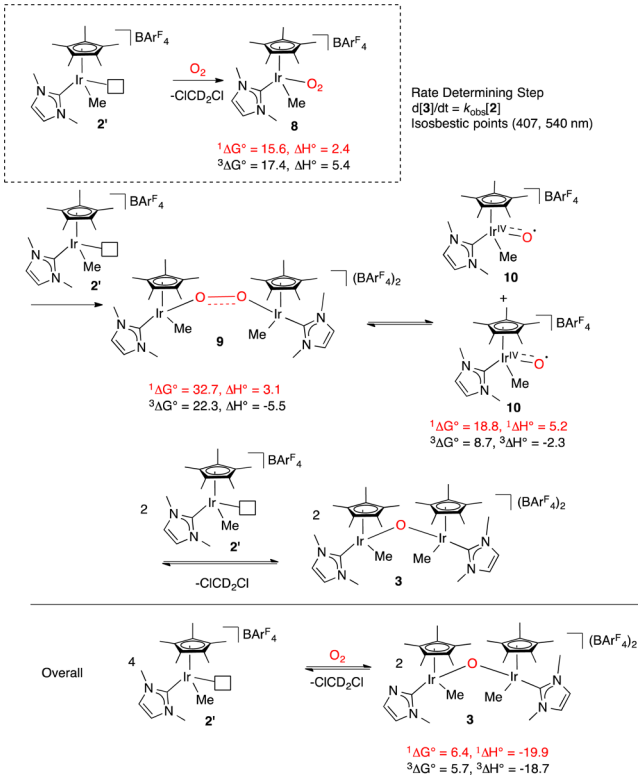

[a]Calculations were performed at the DFT(PBE0) level with the solvent free 16-electron intermediate, cation, [Cp*Ir(NHC)Me$^+$], **2′**. See Computational Methods for details. Reported energies are in kcal/mol. Singlet energies are in red font.

structure of **10** is described below. Complex **10** subsequently reacts with another molecule of complex **2** to generate **3**. Thus, for the overall chemical reaction, four molecules of **2** are required for each dioxygen molecule.

As noted below, the electronic structure for complexes such as **3** and **10** are not accurately described by single determinant DFT methods. Further, several of the transition states have not been located. As a result, the proposed mechanism in Scheme 9 is tentative at this time. However, the mechanism highlights the existence of potentially important intermediates such as the μ-peroxo complex **9** that may precede the formation of iridium oxo/oxyl intermediates.

Electronic Structure of 3. Insights into the unique reactivity of **3** were obtained by an analysis of the bonding in this complex. As noted earlier, **3** was assigned on the basis of its spectroscopic signature as an unusual Ir^{IV}−O−Ir^{IV} complex whereby two d^5 Ir(IV) centers are strongly coupled by the bridging oxo ligand. In a previous report on (xylyl)$_3$Ir−O−Ir(xylyl)$_3$, it was suggested from DFT studies that the diamagnetic nature of the complex is a result of the interaction of the d_z^2 orbitals on both metals with the s and p orbitals on the bridging oxygen.[14a] This was evident in the frontier molecular orbitals, which revealed a significant HOMO−LUMO gap (2.5 eV) and was proposed to account for the diamagnetism of the complex. The structure of **3** can be similarly described by the formulation (X$_3$)Ir^{IV}−O−Ir^{IV}(X$_3$), although the bonding pattern may differ due to the nonlinear arrangement about the μ-oxo.

DOI: 10.1021/ja512905t
J. Am. Chem. Soc. 2015, 137, 3574−3584

At the DFT level of theory, **3** is calculated to have a triplet ground state, but a singlet state is calculated to be only 0.7 kcal/mol higher in energy. Note that several conformations generated by twisting of the C−Ir−Ir−C dihedral were evaluated for singlet and triplet **3**, and the results below are for the lowest energy conformations computed. Triplet **3** has average computed Ir−Me bonds of 2.10 Å, Ir−O bonds of 1.93 Å, an Ir−O−Ir angle of 160°, and a C−Ir−Ir−C dihedral angle of −67°; the singlet analog has average Ir−Me bonds of 2.09 Å, Ir−O bonds of 1.91 Å, an Ir−O−Ir angle of 150°, and a C−Ir−Ir−C dihedral angle of −72°. The DFT computed metric values are thus in excellent agreement with the solid-state structure of **3** (see Figure 2), particularly for the singlet with respect to the Ir−O−Ir bond angle and the C−Ir−Ir−C dihedral angle.

Although the structural differences between singlet and triplet models of **3** are not large, the differences in the calculated UV−vis spectra are larger (see Supporting Information). The calculated UV−vis spectrum further supports the contention that the singlet structure is the true minimum. Furthermore, these computational results are consistent with the diamagnetic nature of complex **3** as observed by its well-defined NMR spectrum.

Although calculations at the DFT level of theory suggest that the singlet and triplet spin states lie within 1 kcal/mol, with the triplet marginally lower, it was expected that coupling between the formally d^5 Ir(IV) centers may be better described with MCSCF (multiconfiguration SCF) than single-determinant DFT methods, so MCSCF computations on a slightly simpler model (where methyl substituents on the Cp* and NHC ligands were replaced with hydrogen, **3′**) were performed. The MCSCF computations (10-orbital, 10-electron CASSCF (complete active space SCF) show the singlet state to be significantly lower in energy by ∼17 kcal/mol than triplet **3′**, consistent with a diamagnetic ground state as inferred from the spectroscopy of **3**.[20]

In addition, the important MCSCF natural orbitals for complex **3′** are informative with respect to the nature of the bonding across the Ir−O−Ir moiety and are depicted in Figure 5. These frontier orbitals show significant delocalization among

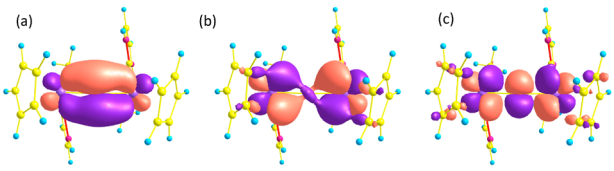

Figure 5. (a) Bonding, (b) nonbonding, and (c) antibonding Ir dπ − O pπ − Ir dπ natural orbitals of **3′** obtained from MCSCF calculations. Natural orbital occupation numbers are 1.93, 1.87, and 0.21 e-, respectively.

the three atoms of the Ir−O−Ir core. The orbital arrangement is quite different from the orbital model put forth for the linear $(xylyl)_3Ir-O-Ir(xylyl)_3$ by Brown et al.,[14a] likely due in part to the nonlinearity about the bridging oxo of **3**. The frontier orbitals indicate strong coupling between iridium centers, supporting the formulation of **3** as $Ir^{IV}-O-Ir^{IV}$. Indeed, the frontier orbitals are reminiscent of bonding in a 3-center, 4-electron allyl anion with bonding (π_b, Figure 5a), nonbonding (π_n, Figure 5b) and antibonding (π_a, Figure 5c) components. The significant departure of natural orbital occupation numbers from ideal values of 0 and 2 e^- ($\pi_b^{1.93}\pi_n^{1.87}\pi_a^{0.21}$) highlights significant multiconfiguration character for the diamagnetic, singlet μ-oxo complex **3**.

The complex $(xylyl)_3Ir-O-Ir(xylyl)_3$ was synthesized from the partial oxygen atom transfer from the Ir^V-oxo species, $(xylyl)_3Ir^V{=}O$ to $(xylyl)_3Ir$.[14a] The formation of **3** can be envisioned from a similar reaction between $[Cp^*Ir(NHC)Me]^+$ and the putative metal oxo $[Cp^*Ir{=}O(NHC)Me]^+$ (Scheme 10). Similar to the bonding model formulated by Wolczanski

Scheme 10. Proposed Mechanism for the Formation of 3 from a Putative Ir^V oxo/oxyl Intermediate

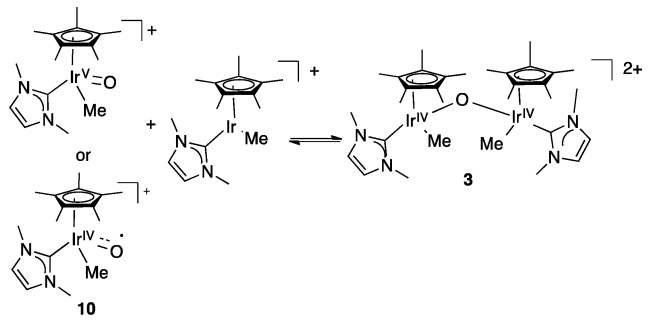

and co-workers[21] for oxygen-atom transfer to/from nitrosyl complexes, orbital symmetry requirements yield a nonlinear arrangement for the oxygen transfer and σ/π mixing, as can be seen in the frontier orbitals that are orthogonal to those depicted in Figure 5 (see Figure 6).[21]

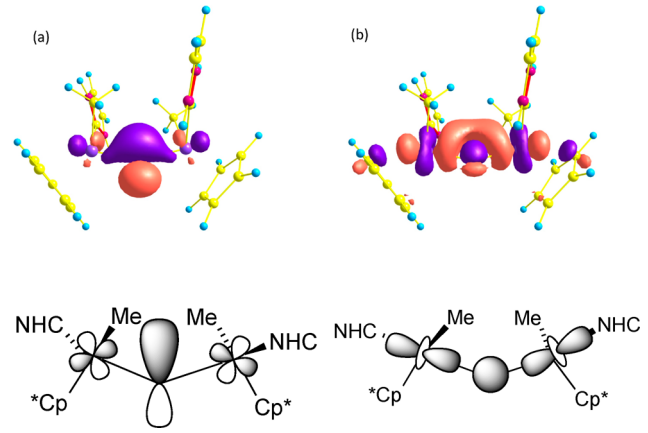

Figure 6. MCSCF frontier orbitals (top) and their cartoon representation (bottom) of **3′** showing σ/π mixing along the IrOIr core. These orbitals lie in the plane perpendicular to that plotted in Figure 5

Electronic Structure of Oxo Iridium Intermediates. It has been suggested in previous studies that d^5 $Ir^{IV}-O-Ir^{IV}$ d^5 species such as **3** may exist in equilibrium with putative Ir oxo/oxyl intermediates.[14a] In addition, Cp*Ir(V) oxo species have been postulated recently in catalytic systems for the hydroxylation of hydrocarbons and water oxidation.[8d,f−h] Although the Cp*Ir oxo species were not isolated, understanding the electronic structure of proposed Cp*Ir oxo intermediates is important for the design of new catalysts. Singlet, $[Cp^*Ir^V{=}O(NHC)Me]^+$, and triplet, $[Cp^*Ir^{IV}{=}O(NHC)Me]^+$, species were calculated. As shown in Scheme 11, the triplet species is 10.1 kcal/mol more stable than the corresponding singlet species by DFT.

DOI: 10.1021/ja512905t
J. Am. Chem. Soc. 2015, 137, 3574−3584

Scheme 11. Relative Energies of ^{1}[Cp*Ir^V=O(NHC)Me]$^+$ and ^{3}[Cp*Ir^{IV}=O(NHC)Me]$^+$

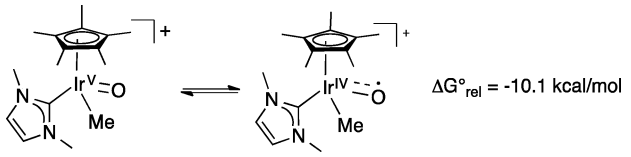

The location of spin density for ^{3}[Cp*Ir^{IV}=O(NHC)Me]$^+$ was calculated with unrestricted DFT methods to understand the nature of the Ir−O multiple bond in this species. The spin density is localized primarily on the Ir (0.76 e-) and oxygen (1.02 e$^-$) atoms with a little spin density on one carbon atom of the Cp* ligand (0.13 e$^-$) (see Supporting Information).

The Ir−O bond length in [Cp*Ir^{IV}=O(NHC)Me$^+$] was calculated to be 1.800 Å. In contrast, the Ir−O bond length in [Cp*Ir^V(=O)(NHC)Me$^+$] was calculated to be 1.794 Å. These data suggest that in both species, there is Ir−O multiple bonding because the bond lengths in both species are shorter than typical Ir−O single bonds (~2.11(8) Å).[22]

Given the multireference character of **3′** and the delocalization of the spin density in the plotted DFT orbitals, an MCSCF treatment of the singlet and triplet states of the monometallic oxo/oxyl complex was deemed prudent. A similar truncation of the methyl groups was performed giving [CpIr(O)(NHC′)-Me]$^+$. Interestingly, a larger active space was necessary (14-orbital, 14-electron CASSCF) for the monomeric Ir complexes as compared with that for **3′**. The calculations also predict a triplet ground state for the monometallic species, but the CASSCF calculations predict only a 4.3 kcal/mol difference between the singlet and triplet states. Inclusion of second-order perturbation at this level of theory (MCQDPT2) showed the triplet to be the ground state by 5.6 kcal/mol.

Important natural orbitals for Ir−O bonding in the singlet (Figure 7) and triplet states (Figure 8) are depicted. For the singlet, there is one σ-bonding orbital and one π-bonding orbital, as would be expected in a typical double bond. There is also significant deviation of the natural orbital occupancy for the singlet from single-determinant values ($\sigma^{1.94}\pi^{1.86}\pi^{*0.15}\sigma^{*0.07}$) indicating multireference character.

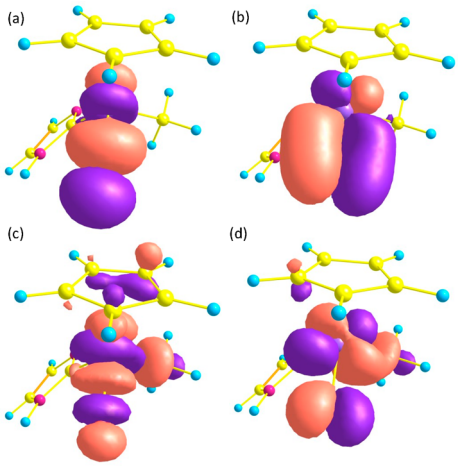

Figure 7. (a) σ-Bonding and (b) π-bonding natural orbitals and (c) σ-antibonding and (d) π-antibonding natural orbitals of [CpIr^V=O(NHC′)Me]$^+$. Natural orbital occupation numbers are 1.94, 1.86, 0.07, and 0.15 e$^-$, respectively.

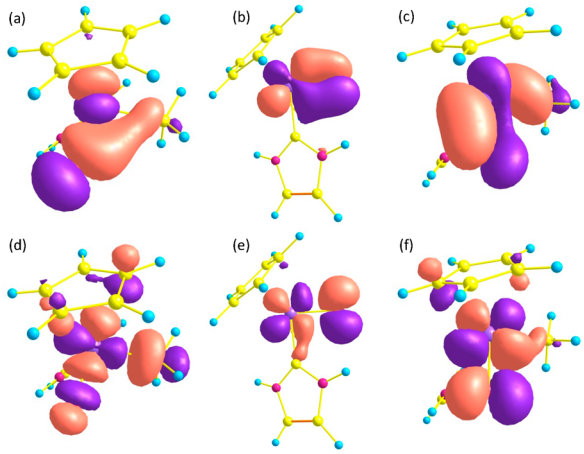

Figure 8. (a) σ-bonding and (b,c) π-bonding and (d) σ-antibonding and (e,f) π-antibonding natural orbitals of ^{3}[CpIr^{IV}=O(NHC′)Me]$^+$. Natural orbital occupation numbers are 1.94, 1.95, 1.95, 0.07, 1.04, and 1.04 e$^-$, respectively.

The triplet state has two Ir−O π-bonding natural orbitals, one primarily Ir$_d$−O$_p$ (Figure 8b), and the second, Ir$_d$−O$_p$ with contributions from Ir−Me and Ir−NHC bonding orbitals (Figure 8c). The Ir−O σ-bonding orbital now also has contributions from the methyl and NHC ligands. The two unpaired electrons occupy two π-antibonding natural orbitals, yielding a pair of orthogonal 3-electron/2-center bonds (Figure 8e and 8f). One of the π-antibonding natural orbitals also has a small contribution from the Cp ring, which corresponds to the spin density calculated by the DFT methods (see Supporting Information).

Proposed Mechanism for Methanol Formation. A mechanism consistent with all of the data is shown in Scheme 12). Chloride abstraction from **1** by NaBAr$^F_4$ leads to **2**. Exposure of this complex to O_2 results in the formation of **10**, which subsequently reacts with another equivalent of **2** to form **3**. Kinetic studies suggest that for the activation of dioxygen, the initial reaction of **2** with O_2 is rate-determining because the rate law for this reaction shows a first-order dependence on **2** and the presence of isosbestic points in the scan of the UV−vis spectrum suggests that intermediates do not accumulate in appreciable concentrations. The activation of O_2 by **2** (1st step Scheme 9) is nonradical in nature and should not be inhibited by radical traps. Indeed, the ^{1}H NMR spectrum of **2** was unaffected by the presence of 1 equiv of TEMPO or 1,4-cyclohexadiene. Further, the same observed rate constant (k_{obs} = 1.2 × 10^{-2} s^{-1}) for the formation of **3** from **2** in the presence and absence of TEMPO was observed.

Methanol formation occurs after the formation of **3**. As suggested by previous reactions with (xylyl)$_3$Ir−O−Ir(xylyl)$_3$ by Brown and co-workers, **3**, **2**, and **10** are expected to exist in equilibrium. The formation of the Ir−OMe intermediate, **5**, results from migration of the methyl ligand to the oxo ligand in **10**. Treatment of this species with ethanol results in alkoxide exchange to generate the Ir−OEt species, **6**.[23] β-hydride elimination results in the formation of the hydride, [Cp*Ir-(NHC)H][BAr$^F_4$], **7** and acetaldehyde. This complex undergoes metathesis with the methylene chloride solvent to form **4**.[24]

The mechanism presented above includes the observed iridium intermediate **3**. Kinetic studies suggest that **3** is an important intermediate in this reaction. The presence of **7** is

DOI: 10.1021/ja512905t
J. Am. Chem. Soc. 2015, 137, 3574−3584

Scheme 12. Proposed Mechanism for Methanol Formation

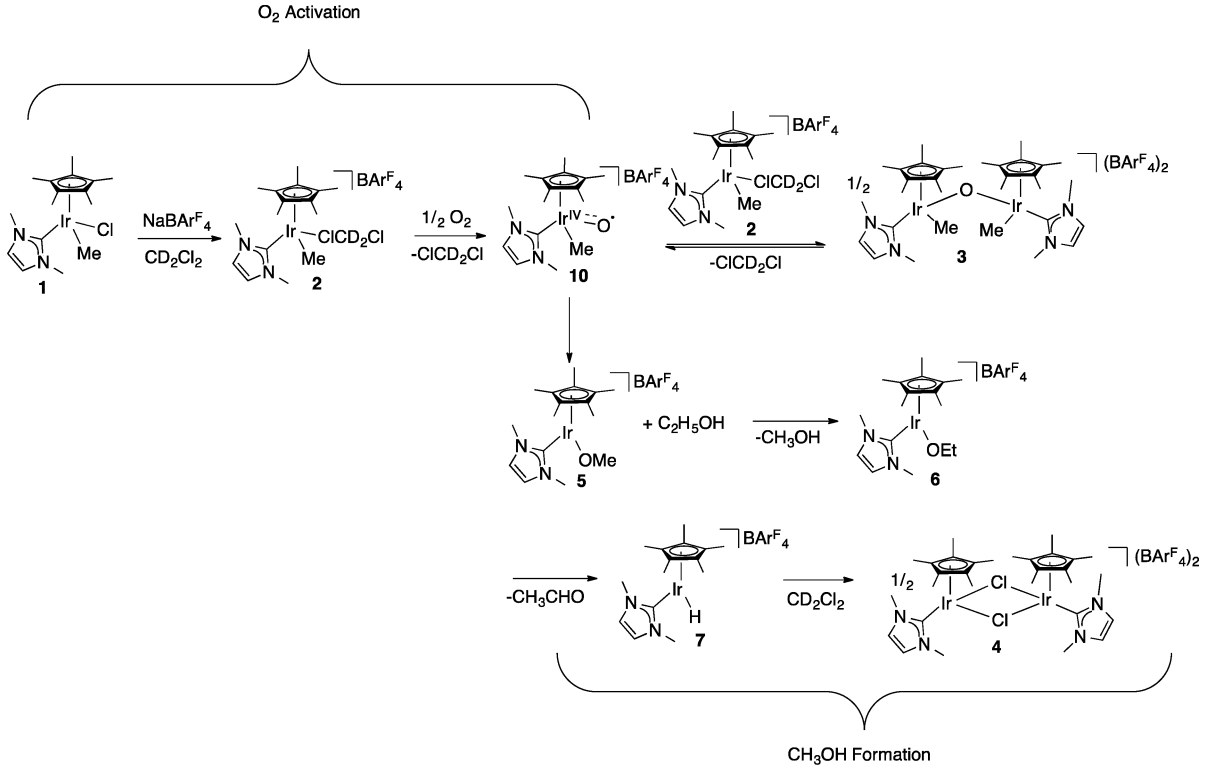

implied by the quantitative observation of acetaldehyde by ^{1}H NMR spectroscopy and the isolation and characterization of **4** in quantitative yields. Isotope labeling experiments confirm that the Ir-Me bond is oxidized to form the methanol product. Importantly, the isolation of **4** suggests that the Cp* and NHC ligands are not oxidized significantly under reaction conditions.

CONCLUSIONS

Methanol formation from Cp*Ir^{III}(NHC)Me complexes was shown to occur quantitatively at room temperature with air (O_2) as the oxidant and ethanol as a proton source. A rare example of a diiridium bimetallic complex, **3**, has been isolated and characterized by ^{1}H and ^{13}C NMR spectroscopy, UV−vis spectroscopy, X-ray crystallography, and both DFT and MCSCF computations. Complex **3** contains a Ir^{IV}−O−Ir^{IV} core whereby two d^5 Ir(IV) centers are bridged by an oxo ligand. Insights into the electronic structure of this intermediate were provided by computational studies, which suggest that the μ-oxo bridge facilitates electronic communication between the iridium centers. Evidence for 3-center, 4-electron bonding reminiscent of an allyl anion was obtained from MCSCF calculations for the μ-oxo intermediate, which experiments show to be a kinetically competent intermediate in the production of methanol by the reaction of dioxygen with these iridium-methyl complexes. Further, these studies suggest that similar to the bonding model formulated by Wolczanski and co-workers,[21] orbital symmetry requirements yield a nonlinear arrangement for the oxygen transfer and σ/π mixing. Obviously, obtaining the desired nonlinear M−O−M arrangement for oxygen atom transfer can be thwarted by utilizing ligands that are less sterically demanding, suggesting that identification of ligand sets that permit nonlinear M−O−M arrangements is a key design element in this oxyfunctionalization chemistry and hence related alkane oxidation catalysis.

Complex **3** likely results from an oxygen atom transfer reaction of **2** with a Cp*Ir oxo intermediate. The electronic structure of this monometallic oxo intermediate was also investigated computationally. MCSCF calculations suggest that the Ir-oxo intermediate may be described by two species that are close in energy and therefore accessible under reaction conditions: a singlet Ir^V−oxo intermediate and a triplet Ir^{IV} oxyl intermediate. Both species have formal Ir−O bond orders of 2; however, their electronic structures are quite different. Bonding in the Ir^V-oxo is reminiscent of the VB description of formaldehyde by Harding and Goddard and the $^1\Delta_g$ state of O_2.[25] The triplet Ir^{IV}−oxyl is more akin to the double bond in the triplet ground state ($^3\sum_g^-$) of dioxygen.[26] As one might expect, these differences in electronic structure imply different manifolds of reactivity.

Ir-oxo/oxyl complexes have emerged from this research, as well as recent papers as important intermediates in C−O bond formation, C−H bond activation, and water splitting. To our knowledge, apart from Wilkinson's $IrMes_3O$,[27] such entities have eluded crystallographic characterization, and more research to elucidate their reactivity with different organometallic and coordination chemistry supporting ligands is clearly needed. One can infer from the present work that careful attention to their electronic structure will need to go beyond single-determinant DFT methods.

The formation of **3** from **2** is not inhibited by the radical traps TEMPO and 1,4-cyclohexadiene; however, methanol formation from **3** is inhibited by TEMPO. Isotope labeling studies confirmed the origin of the methyl group in the methanol product is the iridium−methyl bond. Isolation of the diiridium-containing product **4** in high yields at the end of the reaction shows that the Cp* and NHC ligands remain bound to the iridium and are not significantly degraded under reaction conditions. Complexes with the Cp*Ir(NHC) motif may be

DOI: 10.1021/ja512905t
J. Am. Chem. Soc. 2015, 137, 3574−3584

further developed into a catalytic cycle for the partial oxidation of hydrocarbons. More importantly, the identification of **3** as an intermediate in formation of methanol from dioxygen can provide insight into the activation of transition metal alkyl complexes with O_2 and the subsequent functionalization that results from C−O bond formation. Studies are currently ongoing to understand how the unique electronic properties of **3** influence the oxyfunctionalization of metal−carbon bonds.

EXPERIMENTAL SECTION

General Considerations. Reagents were purchased from commercial sources and used as received. ^{1}H and ^{13}C NMR spectra were recorded on a Varian Mercury 400 MHz or a Varian Mercury 300 MHz spectrometer at room temperature. ^{1}H and ^{13}C NMR chemical shifts are listed in parts per million (ppm) and are referenced to residual protons or carbons of the deuterated solvents, respectively. Elemental analyses were performed by Atlantic Microlabs, Inc. X-ray crystallography was performed at the X-ray Structural Facility of North Carolina State University by Dr. Roger Sommer.

Cp*Ir(NHC)MeCl, 1. In a 25 mL Schlenk flask, Cp*Ir(NHC)Cl_2 (NHC = 1,3,-dimethylimidazol-2-ylidene) (250 mg, 0.505 mmol) was allowed to stir in THF for 10 min. This solution was frozen in a liquid N_2 bath under a stream of N_2. $Zn(Me)_2$ (252 uL, 1.2 M in toluene) was added to the flask under a stream of N_2. The flask was sealed, and the solution was allowed to stir for 20 min. Solvent was removed in vacuo to leave a yellow oil. Subsequent addition of pentane afforded a yellow powder of Cp*Ir(NHC)MeCl (184 mg, 79% yield). ^{1}H NMR (400 MHz, CD_2Cl_2, δ): 0.81 (s, 3H, Ir−Me), 1.61 (s, 15H, Cp*), 3.53 (bs, 3H, N−Me), 3.94 (bs, 3H, N−Me), 6.98 (bs, 2H, CH). ^{13}C NMR (100 MHz, CD_2Cl_2, δ): 161.2, 122.3, 87.9, 8.8, −16.2.

[(Cp*Ir(NHC)Me)$_2$(μ-O)][(BAr$^F_4$)$_2$], 3. In the glovebox, **1** (25 mg, 0.053 mmol) and NaBAr$^F_4$ (94 mg, 0.11 mmol) were added to an ∼20 mL scintillation vial with 5 mL of CH_2Cl_2. The solution was allowed to stand for 30 min. Ten milliliters of pentane was then added to the vial, and the sample was sealed and removed from the glovebox. The vial was then opened to the air, immediately sealed, and left in the freezer at −30 °C for at least 5 h. The blue crystalline product was removed from the vial, washed with excess pentane, and dried in vacuo. The remaining crystals were collected as [(Cp*Ir(NHC)Me)$_2$(μ-O)][(BAr$^F_4$)$_2$] (98 mg, 71% yield). ^{1}H NMR (400 MHz, CD_2Cl_2, δ): 2.11 (s, 15H, Cp*), 3.13 (s, 3H, Ir−Me), 2.96 (s, 3H, N−Me), 3.63 (s, 3H, N−Me), 7.91 (d, J_{HH} = 4 Hz, 1H, CH), 7.88 (d, J_{HH} = 4 Hz, 1H, CH). ^{13}C NMR (100 MHz, CD_2Cl_2, δ): 135, 126.2, 123.4, 117.7, 110.8, 8.3. Anal. Calcd for $C_{96.45}H_{76.90}Cl_{0.9}B_2F_{48}Ir_2N_4O$: C, 43.59; H, 2.92; N, 2.11. Found: C, 43.20; H, 2.90; N, 2.15.

Cp*Ir(NHC)CD$_3$Cl, 1-CD$_3$. In a Schlenk tube, CD_3MgI (0.535 mL, 0.535 mmol, 1 M in ether) was added to a 10 mL THF solution of Cp*Ir(NHC)Cl_2 (NHC = 1,3,-dimethylimidazol-2-ylidene) (250 mg, 0.505 mmol). The solution was allowed to stir for 1 h. The reaction was quenched with water, and the product was extracted with methylene chloride. Solvent was removed in vacuo to leave a yellow oil. Subsequent addition of pentane afforded a yellow powder of Cp*Ir(NHC)-CD_3Cl (165 mg, 69% yield). ^{1}H NMR (400 MHz, CD_2Cl_2, δ): 1.72 (s, 15H, Cp*), 3.61 (s, 3H, N−Me), 3.89 (s, 3H, N−Me), 7.00 (bs, 1H, CH), 6.84 (bs, 1H, CH). ^{13}C NMR (100 MHz, CD_2Cl_2, δ): 158.7, 122.2, 88.6, 9.3.

Synthesis of 3-CD$_3$. In the glovebox, **1-CD$_3$** (25 mg, 0.052 mmol) and NaBAr$^F_4$ (94 mg, 0.11 mmol) were added to an ∼20 mL scintillation vial with 5 mL of CH_2Cl_2. The solution was allowed to stand for 30 min. Ten milliliters of pentane was then added to the vial and the sample was sealed and removed from the glovebox. The vial was then opened to the air, immediately sealed, and left in the freezer at −30 °C for at least 5 h. The blue crystalline product was removed from the vial, washed with excess pentane, and dried in vacuo. The remaining crystals were collected as [(Cp*Ir(NHC)CD_3)$_2$(μ-O)]-[(BAr$^F_4$)$_2$] (85 mg, 62% yield). ^{1}H NMR (400 MHz, CD_2Cl_2, δ): 2.10 (s, 15H, Cp*), 2.95 (s, 3H, N−Me), 3.62 (s, 3H, N−Me), 7.91 (d, J_{HH} = 4 Hz, 1H, CH), 7.88 (d, J_{HH} = 4 Hz, 1H, CH). ^{13}C NMR (100 MHz, CD_2Cl_2, δ): 135, 126.2, 123.4, 117.7, 110.8, 8.3.

General Procedure for Methanol Formation in CD_2Cl_2 from 1. In an ∼3 mL Schlenk tube, **1** (7.1 mg, 0.015 mmol) was added to a solution containing 0.5 mL of 0.03 M 1,3,5-trimethoxybenzene in CD_2Cl_2 and 0.15 M ethanol. NaBAr$^F_4$ (26.6 mg, 0.03 mmol) was added to initiate the reaction. The solution was allowed to stir open to air for the allotted amount of time. The reaction was then removed from the stir plate, and the crude reaction mixture was then transferred to an NMR tube for ^{1}H NMR analysis.

General Procedures for Methanol Formation in CD_2Cl_2 from 3. In an ∼3 mL Schlenk tube, **3** (7.1 mg, 0.015 mmol) was added to a solution that contained 0.5 mL of 0.03 M 1,3,5-trimethoxybenzene in CD_2Cl_2 and 0.15 M ethanol. The solution was allowed to stir open to air for the allotted amount of time. The reaction was then removed from the stir plate, and the crude reaction mixture was then transferred to an NMR tube for ^{1}H NMR analysis.

Kinetic Studies. General Conditions. An ∼3 mL Schlenk flask was charged with the appropriate amount of **1** or **3** and a stir bar. A standard solution (0.5 mL) of CD_2Cl_2 with 0.03 M 1,3,5-trimethoxybenzene and 0.15 M ethanol was added to the flask. NaBAr$^F_4$ (26.6 mg, 0.03 mmol) was added to initiate the reaction with **1**. The solution was allowed to stir open to air for the allotted amount of time. The reaction was then removed from the stir plate, and the crude reaction mixture was then transferred to an NMR tube for ^{1}H NMR analysis. Each data point is the average of at least two runs. Error bars represent the standard deviation.

Formation of 1. In an NMR tube, **1** (7.1 mg, 0.015 mmol) was added to 0.5 mL of a 0.03 M solution of 1,3,5-trimethoxybenzene in CD_2Cl_2 in the glovebox. The reaction was allowed to stand for 30 min before it was removed from the glovebox. The NMR tube was then exposed to air and immediately placed in the instrument. The sample was analyzed utilizing an array to acquire spectra at continual points over the course of an hour. The yields for **1**, **3**, and iridium total (**1** + **3**) were calculated vs the 1,3,5-trimethoxybenzene internal standard.

Formation of 1 in the Presence of TEMPO and 1,4-Cyclohexadiene. In an NMR tube **1** (7.1 mg, 0.015 mmol) was added to a 0.5 mL solution of 0.03 M 1,3,5-trimethoxybenzene and 0.03 M TEMPO in CD_2Cl_2 in the glovebox. The reaction was allowed to stand for 30 min before it was removed from the glovebox. The NMR tube was then exposed to air and immediately placed in the instrument. The sample was analyzed utilizing an array to acquire spectra at continual points over the course of an hour. The yields for **1**, **3**,

DOI: 10.1021/ja512905t
J. Am. Chem. Soc. 2015, 137, 3574−3584

and iridium total (**1** + **3**) were calculated vs the 1,3,5-trimethoxybenzene internal standard.

Eyring Plots. To obtain Eyring plots, reactions were run under the general conditions outlined above at 0, 10, and 25 °C. At 0 °C, the temperature was maintained by running the reactions in an ice bath. For the data at 10 °C a 1,4-dioxane/liquid N_2 bath was used to maintain a constant temperature. At the lower temperature, the standard solutions were cooled to the appropriate temperature before the reaction was initiated.

Computational Methods. DFT calculations were performed using the Gaussian 09 suite of programs.[28] Structures were optimized with the PBE0[29] hybrid/exchange functional. For iridium, the Stuttgart[30] pseudopotential with a triple-ζ level valence and *f* polarization function (exponent = 0.685). For all other elements, a 6-311G** basis set was used. Optimizations were performed with implicit solvation of methylene chloride (ε = 8.93) by the SMD[31] method, and dispersion effects were included using Grimme's D3 dispersion correction with Becke–Johnson damping.[32] Structures were identified as minimum or transition states by the presence of zero or one imaginary frequency in the energy Hessian.

MCSCF[33] and MCQDPT2[34] were performed on truncated systems on the optimized DFT structures using the GAMESS[35] program. For these multireference calculations, no dispersion or solvent corrections were considered. For the bimetallic systems a (10,10) active space was chosen and for monometallic complexes a (14,14) active space with second-order perturbation theory was chosen on the basis of convergence of the singlet–triplet energy gaps.

■ ASSOCIATED CONTENT

Supporting Information

Additional experimental procedures for methanol formation, isotopic labeling and kinetic studies. X-ray experimental for **3** and **4**. Full Gaussian reference and coordinates for key intermediates. This material is available free of charge via the Internet at http://pubs.acs.org.

■ AUTHOR INFORMATION

Corresponding Author

*E-mail: eaison@ncsu.edu

Notes

The authors declare no competing financial interests.

■ ACKNOWLEDGMENTS

This work was supported by the NSF as part of the Center for Enabling New Technologies through Catalysis (CENTC), CHE-0650456 and CHE-1205189. We thank Karen I. Goldberg, William D. Jones, and Melanie S. Sanford for helpful discussions.

■ REFERENCES

(1) (a) Boisvert, L.; Goldberg, K. I. *Acc. Chem. Res.* **2012**, *45* (6), 899–910. (b) Company, A.; Lloret, J.; Gomez, L.; Costas, M. *Catal. Met. Complexes* **2012**, *38*, 143–228. (c) Golisz, S. R.; Gunnoe, T. B.; Goddard, W. A., III; Groves, J. T.; Periana, R. A. *Catal. Lett.* **2011**, *141* (2), 213–221. (d) Cai, X.-C.; Majumdar, S.; Fortman, G. C.; Cazin, C. S. J.; Slawin, A. M. Z.; Lhermitte, C.; Prabhakar, R.; Germain, M. E.; Palluccio, T.; Nolan, S. P.; Rybak-Akimova, E. V.; Temprado, M.; Captain, B.; Hoff, C. D. *J. Am. Chem. Soc.* **2011**, *133* (5), 1290–1293. (e) Campbell, A. N.; Stahl, S. S. *Acc. Chem. Res.* **2012**, *45* (6), 851–863. (f) Shi, Z.; Zhang, C.; Tang, C.; Jiao, N. *Chem. Soc. Rev.* **2012**, *41* (8), 3381–3430. (g) Stahl, S. S. *Science* **2005**, *309* (5742), 1824–1826. (h) Wu, W.; Jiang, H. *Acc. Chem. Res.* **2012**, *45* (10), 1736–1748. (i) Olah, G. A. *Angew. Chem., Int. Ed.* **2005**, *44*, 2636–2639.

(2) (a) Bergman, R. G. *Nature* **2007**, *446* (7134), 391–3. (b) Goldman, A. S.; Goldberg, K. I. *ACS Symp. Ser.* **2004**, *885*, 1–43.

(3) (a) Scheuermann, M. L.; Boyce, D. W.; Grice, K. A.; Kaminsky, W.; Stoll, S.; Tolman, W. B.; Swang, O.; Goldberg, K. I. *Angew. Chem., Int. Ed.* **2014**, *53* (25), 6492–6495. (b) Prantner, J. D.; Kaminsky, W.; Goldberg, K. I. *Organometallics* **2014**, *33* (13), 3227–3230. (c) Petersen, A. R.; Taylor, R. A.; Vicente-Hernández, I.; Mallender, P. R.; Olley, H.; White, A. J. P.; Britovsek, G. J. P. *J. Am. Chem. Soc.* **2014**, *136* (40), 14089–14099. (d) Oloo, W. N.; Zavalij, P. Y.; Vedernikov, A. N. *Organometallics* **2013**, *32* (19), 5601–5614. (e) Chuang, G. J.; Wang, W.; Lee, E.; Ritter, T. *J. Am. Chem. Soc.* **2011**, *133* (6), 1760–1762. (f) Denney, M. C.; Smythe, N. A.; Cetto, K. L.; Kemp, R. A.; Goldberg, K. I. *J. Am. Chem. Soc.* **2006**, *128* (8), 2508–2509. (g) Dura-Vila, V.; Mingos, D. M. P.; Vilar, R.; White, A. J. P.; Williams, D. J. *Chem. Commun.* **2000**, *16*, 1525–1526. (h) Jintoku, T.; Nishimura, K.; Takaki, K.; Fujiwara, Y. *Chem. Lett.* **1990**, No. 9, 1687–8. (i) Jintoku, T.; Takaki, K.; Fujiwara, Y.; Fuchita, Y.; Hiraki, K. *Bull. Chem. Soc. Jpn.* **1990**, *63* (2), 438–41. (j) Jintoku, T.; Taniguchi, H.; Fujiwara, Y. *Chem. Lett.* **1987**, No. 9, 1865–8. (k) Konnick, M. M.; Guzei, I. A.; Stahl, S. S. *J. Am. Chem. Soc.* **2004**, *126* (33), 10212–10213. (l) Landis, C. R.; Morales, C. M.; Stahl, S. S. *J. Am. Chem. Soc.* **2004**, *126* (50), 16302–16303. (m) Lyons, T. W.; Sanford, M. S. *Chem. Rev.* **2010**, *110* (2), 1147–1169. (n) Zhang, Y.-H.; Yu, J.-Q. *J. Am. Chem. Soc.* **2009**, *131* (41), 14654–14655.

(4) Look, J. L.; Wick, D. D.; Mayer, J. M.; Goldberg, K. I. *Inorg. Chem.* **2009**, *48* (4), 1356–1369.

(5) (a) Keith, J. M.; Goddard, W. A. *J. Am. Chem. Soc.* **2009**, *131* (4), 1416–1425. (b) Popp, B. V.; Morales, C. M.; Landis, C. R.; Stahl, S. S. *Inorg. Chem.* **2010**, *49* (18), 8200–8207. (c) Popp, B. V.; Stahl, S. S. *Chem.—Eur. J.* **2009**, *15* (12), 2915–2922.

(6) Rostovtsev, V. V.; Henling, L. M.; Labinger, J. A.; Bercaw, J. E. *Inorg. Chem.* **2002**, *41* (14), 3608–3619.

(7) (a) Allen, K. E.; Heinekey, D. M.; Goldman, A. S.; Goldberg, K. I. *Organometallics* **2014**, *33* (6), 1337–1340. (b) Ishikawa, A.; Nakao, Y.; Sato, H.; Sakaki, S. *Inorg. Chem.* **2009**, *48* (17), 8154–8163.

(8) (a) Blakemore, J. D.; Schley, N. D.; Balcells, D.; Hull, J. F.; Olack, G. W.; Incarvito, C. D.; Eisenstein, O.; Brudvig, G. W.; Crabtree, R. H. *J. Am. Chem. Soc.* **2010**, *132* (45), 16017–16029. (b) Brewster, T. P.; Blakemore, J. D.; Schley, N. D.; Incarvito, C. D.; Hazari, N.; Brudvig, G. W.; Crabtree, R. H. *Organometallics* **2011**, *30* (5), 965–973. (c) Codola, Z.; Cardoso, J. M. S.; Royo, B.; Costas, M.; Lloret-Fillol. *J. Chem.—Eur. J.* **2013**, *19* (22), 7203–7213. (d) Hull, J. F.; Balcells, D.; Blakemore, J. D.; Incarvito, C. D.; Eisenstein, O.; Brudvig, G. W.; Crabtree, R. H. *J. Am. Chem. Soc.* **2009**, *131* (25), 8730–8731. (e) Ingram, A. J.; Wolk, A. B.; Flender, C.; Zhang, J.; Johnson, C. J.; Hintermair, U.; Crabtree, R. H.; Johnson, M. A.; Zare, R. N. *Inorg. Chem.* **2014**, *53* (1), 423–433. (f) Zhou, M.; Balcells, D.; Parent, A. R.; Crabtree, R. H.; Eisenstein, O. *ACS Catal.* **2012**, *2* (2), 208–218. (g) Zhou, M.; Hintermair, U.; Hashiguchi, B. G.; Parent, A. R.; Hashmi, S. M.; Elimelech, M.; Periana, R. A.; Brudvig, G. W.; Crabtree, R. H. *Organometallics* **2013**, *32* (4), 957–965. (h) Zhou, M.; Schley, N. D.; Crabtree, R. H. *J. Am. Chem. Soc.* **2010**, *132* (36), 12550–12551.

(9) Williams, D. B.; Kaminsky, W.; Mayer, J. M.; Goldberg, K. I. *Chem. Commun.* **2008**, *35*, 4195–4197.

(10) Lehman, M. C.; Boyle, P. D.; Sommer, R. D.; Ison, E. A. *Organometallics* **2014**, *33* (19), 5081–5084.

(11) Similar to the complex $[Cp^*Ir(PMe_3)(Me)(Ch_2Cl_2)][BAr^F{}_4]$ reported by Bergman and coworkers, the cationic complexes reported here are shown as methylene chloride adducts as the solvent free complexes were shown to be unstable. See: Arndtsen, B. A.; Bergman, R. G. *Science* **1995**, *270*, 1970.

(12) (a) Liu, F.; Concepcion, J. J.; Jurss, J. W.; Cardolaccia, T.; Templeton, J. L.; Meyer, T. J. *Inorg. Chem.* **2008**, *47* (6), 1727–1752. (b) Uemura, S.; Spencer, A.; Wilkinson, G. *Dalton Trans.* **1973**, *23*, 2565–71. (c) Castillo-Blum, S. E.; Richens, D. T.; Sykes, A. G. *Chem. Commun.* **1986**, *14*, 1120–1. (d) Castillo-Blum, S. E.; Richens, D. T.;

DOI: 10.1021/ja512905t
J. Am. Chem. Soc. 2015, 137, 3574–3584

Sykes, A. G. *Inorg. Chem.* **1989**, *28* (5), 954−60. (e) Burford, R. J.; Piers, W. E.; Ess, D. H.; Parvez, M. *J. Am. Chem. Soc.* **2014**, *136* (8), 3256−3263. (f) Hintermair, U.; Sheehan, S. W.; Parent, A. R.; Ess, D. H.; Richens, D. T.; Vaccaro, P. H.; Brudvig, G. W.; Crabtree, R. H. *J. Am. Chem. Soc.* **2013**, *135* (29), 10837−10851. (g) Hintermair, U.; Hashmi, S. M.; Elimelech, M.; Crabtree, R. H. *J. Am. Chem. Soc.* **2012**, *134* (23), 9785−9795. (h) Graeupner, J.; Hintermair, U.; Huang, D. L.; Thomsen, J. M.; Takase, M.; Campos, J.; Hashmi, S. M.; Elimelech, M.; Brudvig, G. W.; Crabtree, R. H. *Organometallics* **2013**, *32* (19), 5384−5390.

(13) McGhee, W. D.; Foo, T.; Hollander, F. J.; Bergman, R. G. *J. Am. Chem. Soc.* **1988**, *110* (25), 8543−8545.

(14) (a) Fortner, K. C.; Laitar, D. S.; Muldoon, J.; Pu, L.; Braun-Sand, S. B.; Wiest, O.; Brown, S. N. *J. Am. Chem. Soc.* **2007**, *129* (3), 588−600. (b) Fortner, K. C.; Laitar, D. S.; Muldoon, J.; Pu, L.; Braun-Sand, S. B.; Wiest, O.; Brown, S. N. *J. Am. Chem. Soc.* **2007**, *129* (3), 588−600.

(15) (a) Cheng, P. T.; Nyburg, S. C. *Inorg. Chem.* **1975**, *14* (2), 327−329. (b) Carty, P.; Walker, A.; Mathew, M.; Palenik, G. J. *J. Chem. Soc. D* **1969**, *23*, 1374−5. (c) Baranovskii, I. B.; Golubnichaya, M. A.; Koz'min, P. A.; Surazhskaya, M. D. *Zh. Neorg. Khim.* **1995**, *40* (10), 1634−40. (d) Ahmed, T. S.; Tonks, I. A.; Labinger, J. A.; Bercaw, J. E. *Organometallics* **2013**, *32* (11), 3322−3326.

(16) (a) Sutherland, B. R.; Cowie, M. *Organometallics* **1985**, *4* (9), 1637−48. (b) Chandrasekhar, V.; Mahanti, B.; Bandipalli, P.; Bhanuprakash, K. *Inorg. Chem.* **2012**, *51* (20), 10536−10547. (c) Panichakul, D.; Su, Y.; Li, Y.; Deng, W.; Zhao, J.; Li, X. *Organometallics* **2008**, *27* (24), 6390−6392. (d) Slaney, M. E.; Anderson, D. J.; Ferguson, M. J.; McDonald, R.; Cowie, M. *J. Am. Chem. Soc.* **2010**, *132* (46), 16544−16558. (e) Ionkin, A. S.; Wang, Y.; Marshall, W. J.; Petrov, V. A. *J. Organomet. Chem.* **2007**, *692* (22), 4809−4827. (f) Dorta, R.; Rozenberg, H.; Shimon, L. J. W.; Milstein, D. *J. Am. Chem. Soc.* **2002**, *124* (2), 188−189. (g) Dorta, R.; Rozenberg, H.; Shimon, L. J. W.; Milstein, D. *Chem.—Eur. J.* **2003**, *9* (21), 5237−5249. (h) Dadci, L.; Elias, H.; Frey, U.; Hoernig, A.; Koelle, U.; Merbach, A. E.; Paulus, H.; Schneider, J. S. *Inorg. Chem.* **1995**, *34* (1), 306−15. (i) Park, J. T.; Nishioka, T.; Suzuki, T.; Isobe, K. *Bull. Chem. Soc. Jpn.* **1994**, *67* (7), 1968−71.

(17) (a) Kownacki, I.; Kubicki, M.; Blazejewska-Chadyniak, P. *Polyhedron* **2013**, *53*, 26−31. (b) Yuan, X.; Zhang, S.; Ding, Y. *Inorg. Chem. Commun.* **2012**, *17*, 26−29. (c) Kownacki, I.; Marciniec, B.; Kubicki, M. *Chem. Commun.* **2003**, *1*, 76−77.

(18) (a) Crabtree, R. H. 2012, *112* (3), 1536−1554;. (b) Park-Gehrke, L. S.; Freudenthal, J.; Kaminsky, W.; DiPasquale, A. G.; Mayer, J. M. *Dalton Trans.* **2009**, *11*, 1972−1983. (c) Thomsen, J. M.; Sheehan, S. W.; Hashmi, S. M.; Campos, J.; Hintermair, U.; Crabtree, R. H.; Brudvig, G. W. *J. Am. Chem. Soc.* **2014**, *136* (39), 13826−13834. (d) Turlington, C. R.; Harrison, D. P.; White, P. S.; Brookhart, M.; Templeton, J. L. *Inorg. Chem.* **2013**, *52* (19), 11351−11360.

(19) Complex **4** with $MeB(C_6F_5)_3^-$ counterions have been previously reported by Heinekey and coworkers: Meredith, J. M.; Robinson, R., Jr.; Goldberg, K. I.; Kaminsky, W.; Heinekey, D. M. *Organometallics* **2012**, *31* (5), 1879−1887.

(20) Calculations on the full model **3** with smaller MCSCF active space and **3′** with larger active spaces all show that the energy of the singlet is less than the triplet.

(21) (a) Veige, A. S.; Slaughter, L. M.; Lobkovsky, E. B.; Wolczanski, P. T.; Matsunaga, N.; Decker, S. A.; Cundari, T. R. *Inorg. Chem.* **2003**, *42* (20), 6204−6224. (b) Veige, A. S.; Slaughter, L. M.; Wolczanski, P. T.; Matsunaga, N.; Decker, S. A.; Cundari, T. R. *J. Am. Chem. Soc.* **2001**, *123* (26), 6419−6420.

(22) The average Ir−O bond length was obtained from 1205 hits in a search of the Cambridge Structural Database

(23) In the presence of proton sources, the species $[Cp^*Ir^{IV}{=}O(NHC)Me][BAr^F{}_4]$ may readily couple with radical traps such as TEMPO and 1,4-cyclohexadiene and prevent formation of **5** and **6**, which are necessary for the formation of the hydride **7**. Alternatively, **7** may react rapidly with the radical traps, resulting in the unfavorable formation of an unknown iridium species and subsequent decomposition of the complex. See, for example: Albéniz, A. C.; Espinet, P.; López-Fernández, R.; Sen, A. *J. Am. Chem. Soc.* **2002**, *124* (38), 11278−11279.

(24) Halide exchange with halogenated solvents is a typical reaction of transition metal hydrides. See, for example: Matano, Y.; Brown, S. N.; Northcutt, T. O.; Mayer, J. M. *Organometallics* **1998**, *17*, 2939−2941. In addition, for a proposed mechanism for the formation of **4** from **7**, see Scheme S2 in the Supporting Information.

(25) Harding, L. B.; Goddard, W. A. *J. Am. Chem. Soc.* **1975**, *97* (22), 6293−6299.

(26) Moss, B. J.; Bobrowicz, F. W.; Goddard, W. A. *J. Chem. Phys.* **1975**, *63* (11), 4632−4639.

(27) Hay-Motherwell, R. S.; Wilkinson, G.; Hussain-Bates, B.; Hursthouse, M. B. *Polyhedron* **1993**, *12* (16), 2009−12.

(28) Frisch, M. J.; Trucks, G. W.; Schlegel, H. B.; et al. *Gaussian 09, Revisions, D.01*; Gaussian, Inc.: Wallingford, CT, 2009.

(29) Adamo, C.; Barone, V. J. *Chem. Phys.* **1999**, *110* (13), 6158−6170.

(30) Andrae, D.; Haeussermann, U.; Dolg, M.; Stoll, H.; Preuss, H. *Theor. Chim. Acta* **1990**, *77* (2), 123−41.

(31) Marenich, A. V.; Cramer, C. J.; Truhlar, D. G. *J. Phys. Chem. B* **2009**, *113* (18), 6378−6396.

(32) Grimme, S.; Ehrlich, S.; Goerigk, L. *J. Comput. Chem.* **2011**, *32* (7), 1456−1465.

(33) Schmidt, M. W.; Gordon, M. S. *Annu. Rev. Phys. Chem.* **1998**, *49*, 233−266.

(34) Chaban, G. M.; Gordon, M. S. *J. Phys. Chem. A* **1999**, *103* (1), 185−189.

(35) Schmidt, M. W.; Baldridge, K. K.; Boatz, J. A.; Elbert, S. T.; Gordon, M. S.; Jensen, J. H.; Koseki, S.; Matsunaga, N.; Nguyen, K. A.; et al. *J. Comput. Chem.* **1993**, *14* (11), 1347−63.

DOI: 10.1021/ja512905t
J. Am. Chem. Soc. 2015, 137, 3574−3584